Electronic Supplementary Material (ESI) for Materials Advances.

Supplementary Information

A robust and high performance copper silicide catalyst for electrochemical CO_2 reduction

Vladislav Dřínek[*a], *Pavel Dytrych*[a], *Radek Fajgar*[a], *Mariana Klementová*[b], *Jaroslav Kupčík*[a], *Jaromír Kopeček*[b], *Petr Svora*[b], *Martin Koštejn*[a], *Věra Jandová*[a], *Karel Soukup*[a], *Radim Beranek*[c]

[a] Institute of Chemical Process Fundamentals of the CAS, v.v.i., Rozvojová 135, 165 02 Prague, Czech Republic

[b] Institute of Physics of the CAS, v.v.i., Na Slovance 2, 182 00 Prague, Czech Republic

[c] Institute of Electrochemistry, Ulm University, Albert-Einstein-Allee 47, 89081 Ulm, Germany

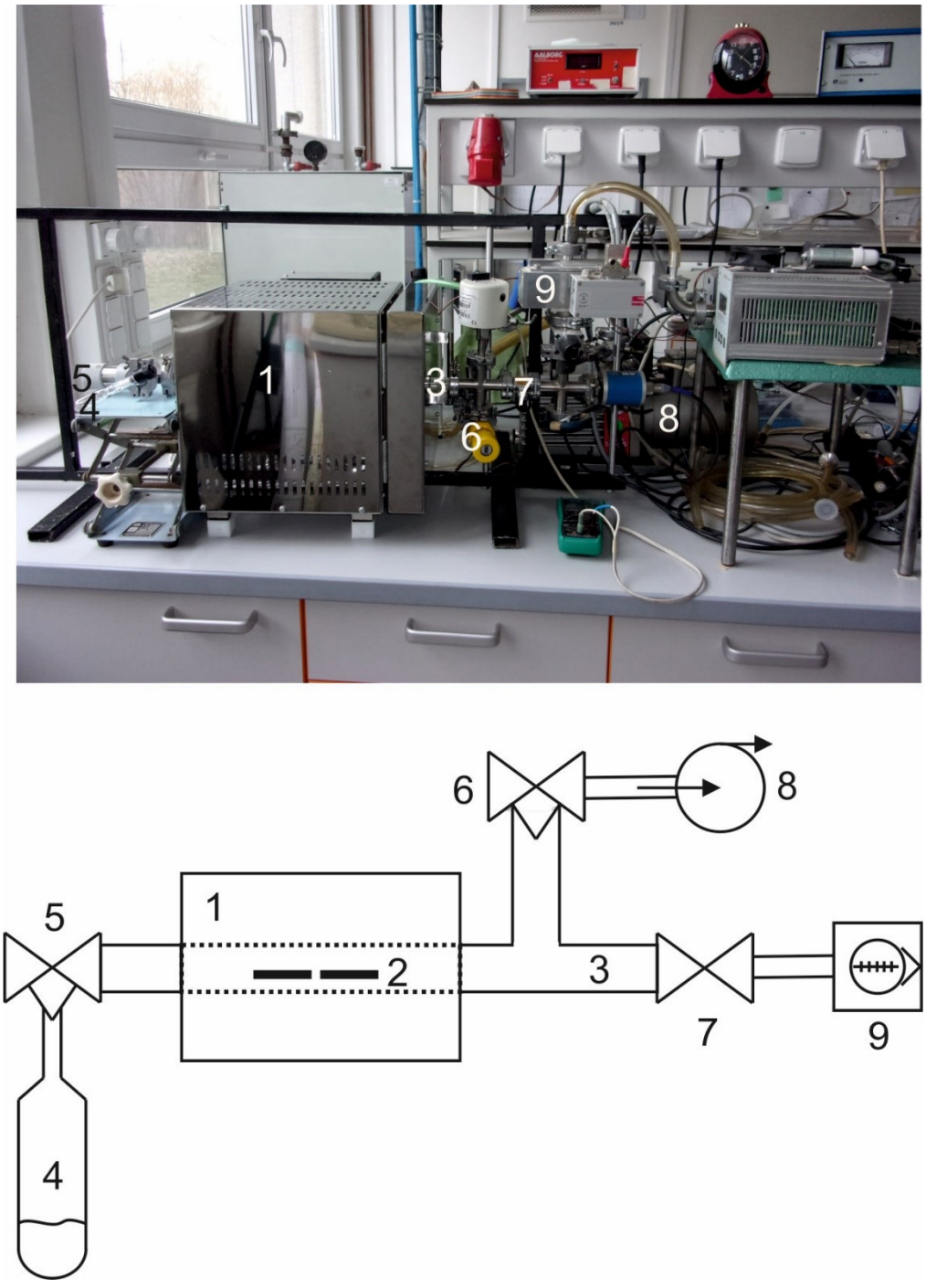

Figure S1 – CVD scheme: 1 – oven, 2 – substrates, 3 – quartz tube, 4 – flask with precursor, 5+6 – needle dosing valve, 7 – gate valve, 8 – rotary pump, 9 – turbomolecular pump

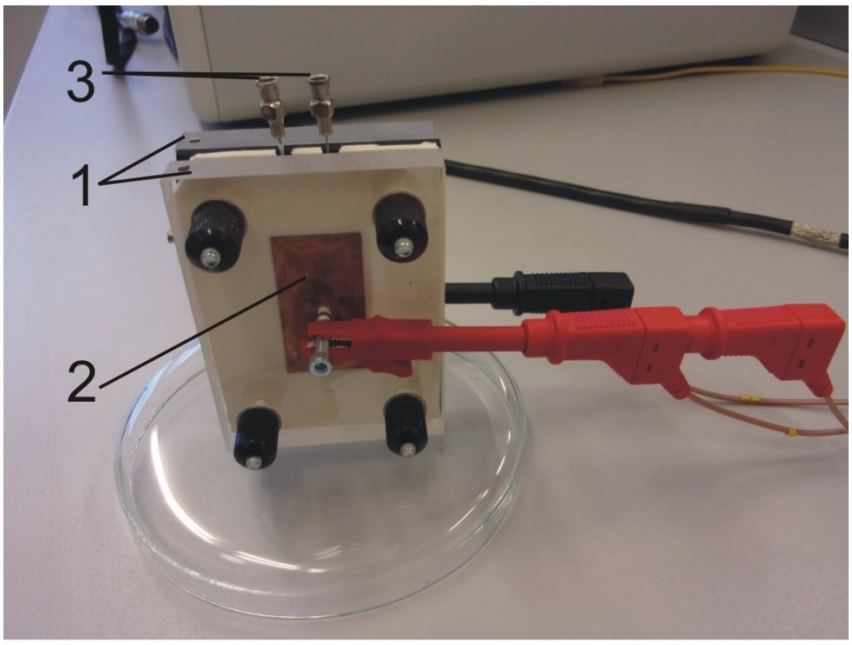

1 Electrolyser
2 Catalyst
3 Electrolyt inlets

Figure S2 – Electrochemical H-cell

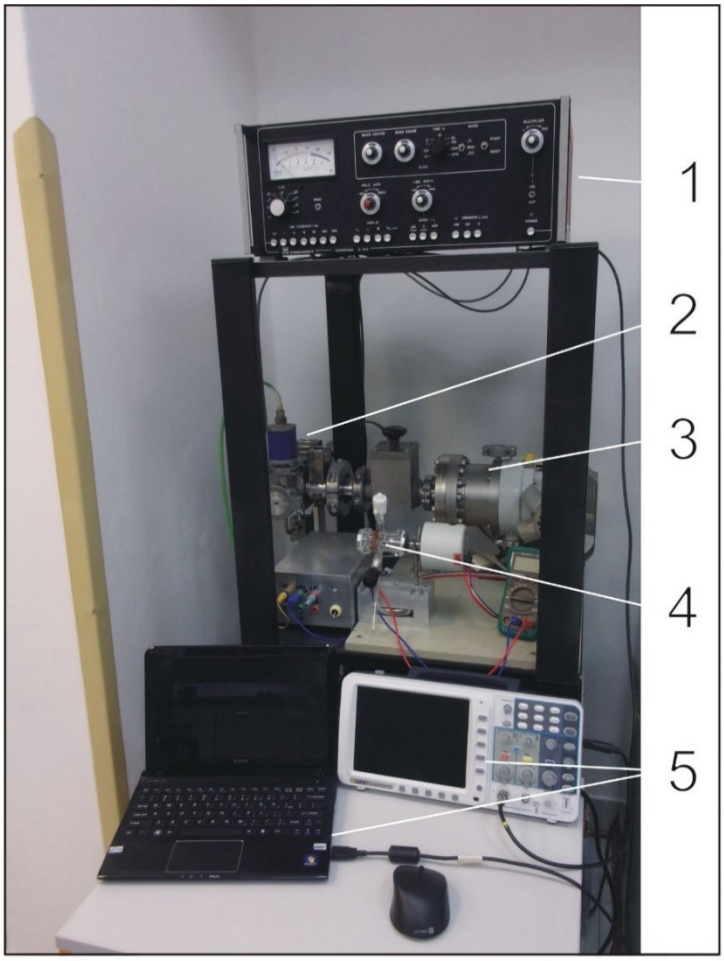

1 Mass spectrometer Quadruvac Q200 (Leybold Heaeus)
2 Mass detector
3 Turbomolecular pump
4 Sample cell
5 Displaying unit (Owon DS8102V/computer)

Figure S3 - On-line mass spectrometer

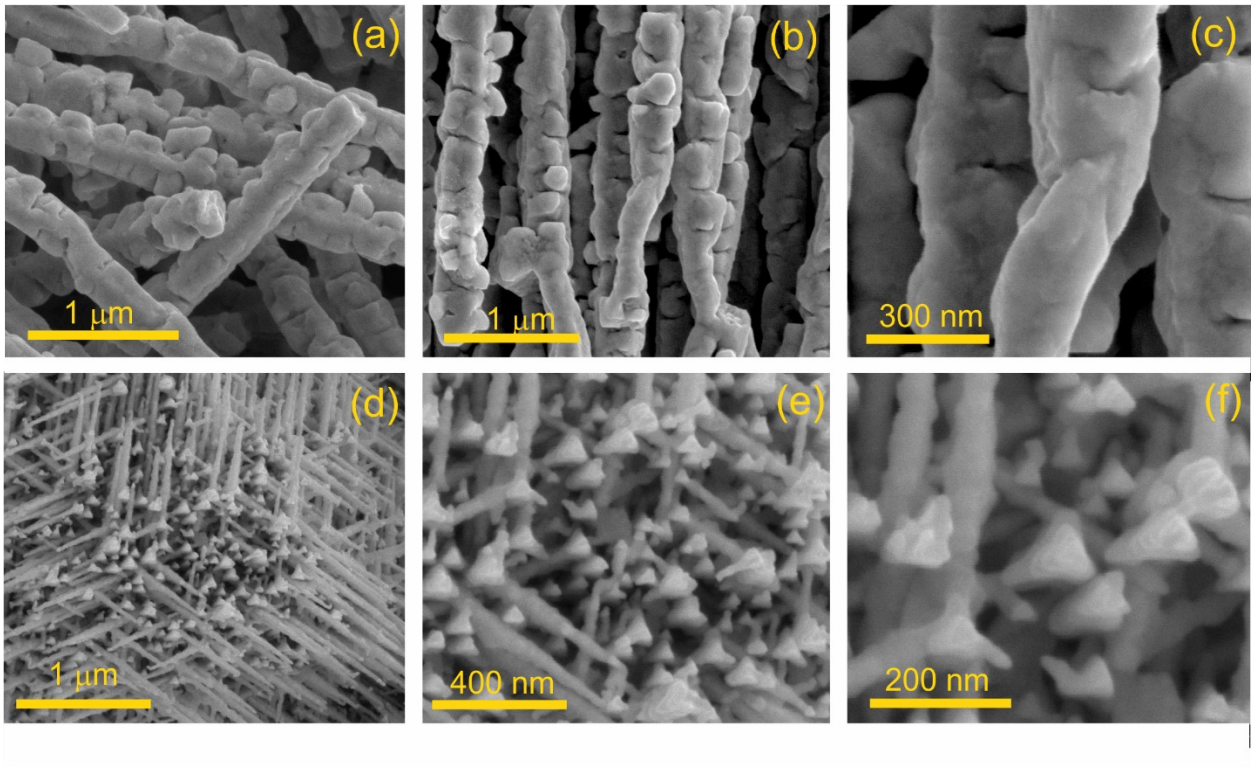

Figure S4 - FESEM images of various objects found in gray-black deposit: a, b, c) nanorods and d, e, f) nanoneedles

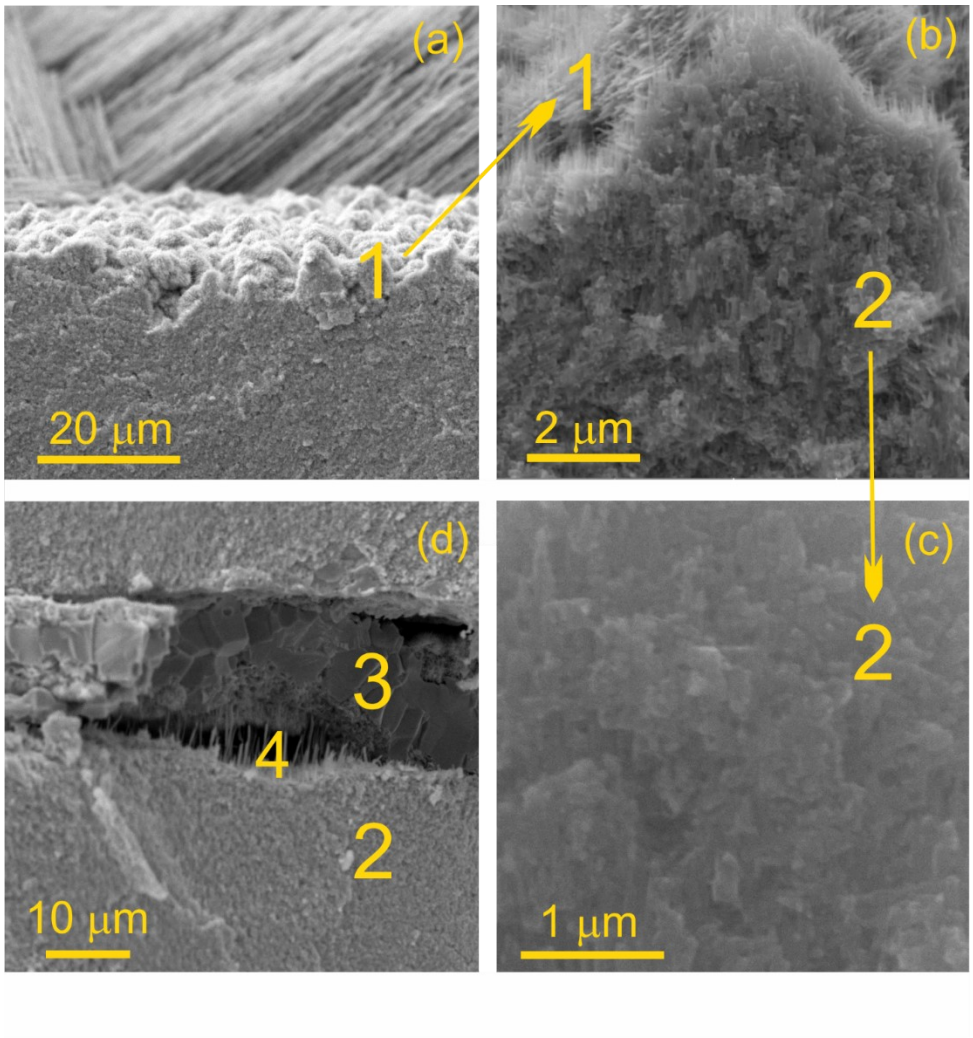

Figure S5 – Partial SEM side views of the broken gray-black Cu_xSi sample: a) boundary between surface nanoobjects (region 1) and the porous, spongy-like matter (region 2), b) detailed view, c) morphology of the spongy mass and d) the middle part of the substrate with the rest of the original copper substrate (region 3) and cavities (region 4) between the copper substrate (region 3) and the spongy mass (region 2).

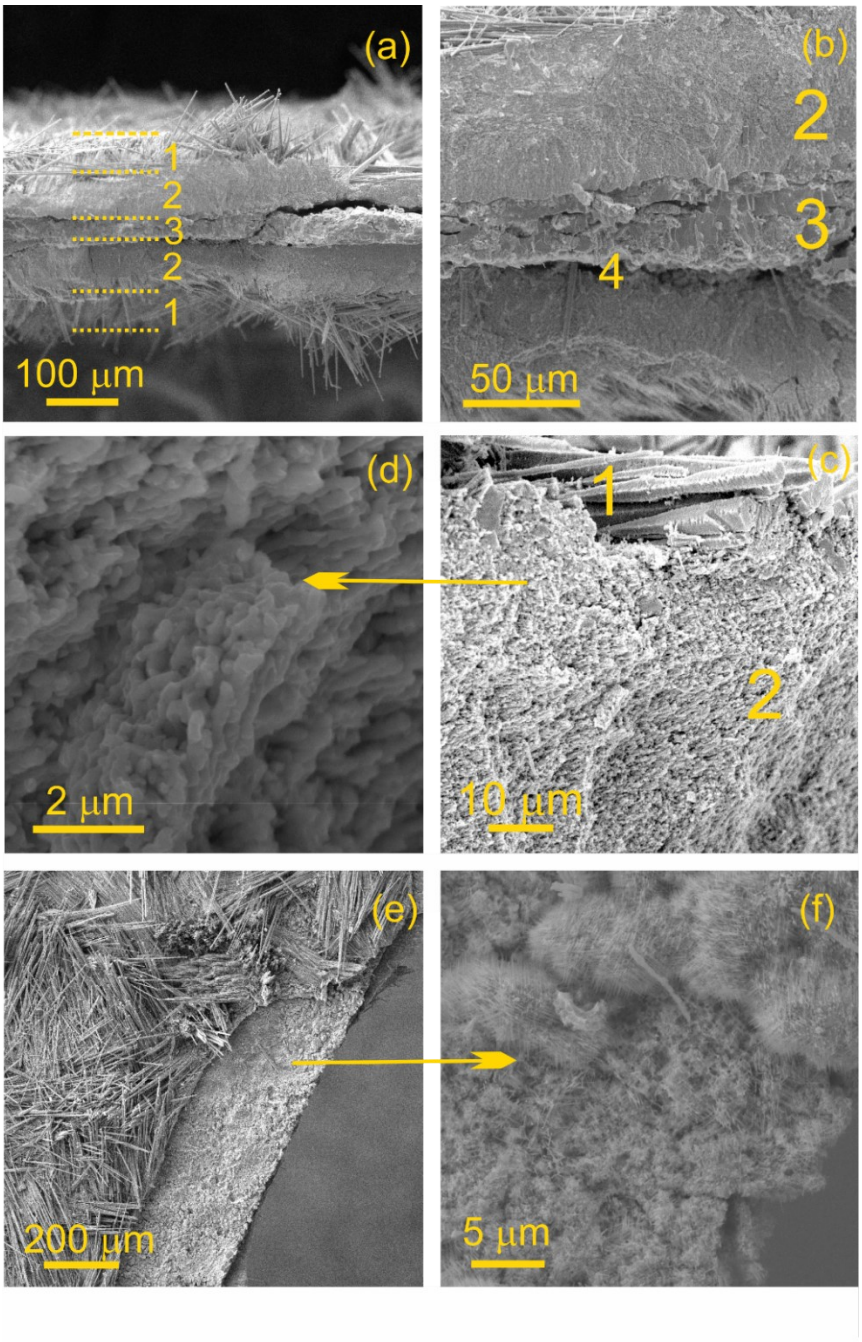

Figure S6 – Images of side views of the broken bluish Cu_xSi sample grown onto 0.1 mm substrate: a) complete side view, thickness of particular regions indicated: surface objects (region 1) – 40-45 µm (on average), the porous, spongy-like layer (2) – 40-60 µm, middle copper part (3) - 40 µm, b) detailed view of a) with cavities (region 4), c) boundary between surface morphology (1) and the porous, spongy-like matter (2), d) detail of the spongy mass, e) sample with unstuck, bare edge part representing the surface of the interface between regions 2 and 3 where the cavities (4) were located and f) morphology of the interface containing nanowires and nanoneedles. Approximate thickness of catalysis driving material is 2x(40µm (region 1)+50µm (region 2))~180 µm.

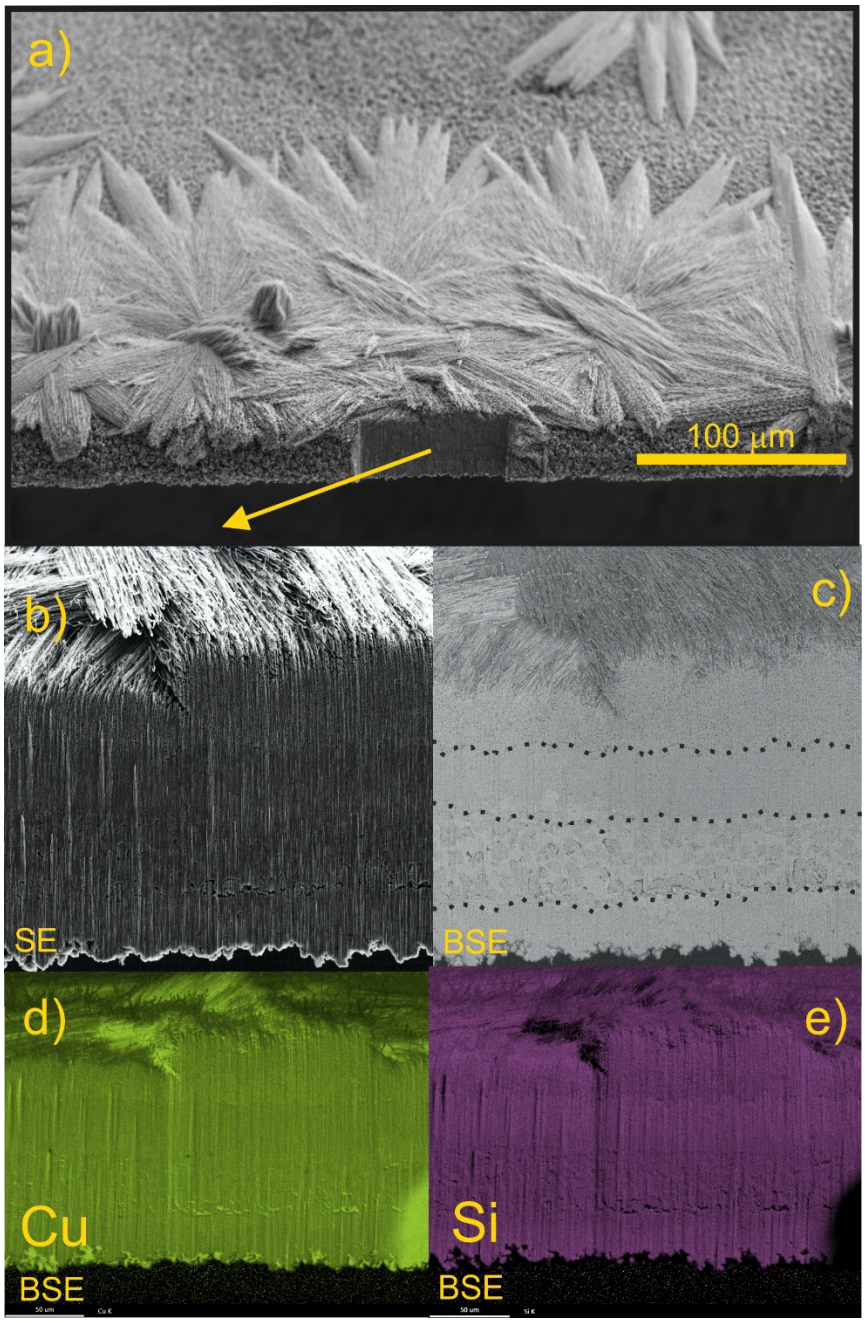

Figure S7 - The whole cross-section of the gray-black deposit formed by FIB in the below part of the image is visible in a). The cross-section; image in b) secondary electrons (SE), c) backscattered secondary electrons (BSE) and elemental mapping in d) copper and e) silicon backscattered secondary electrons. Boundaries of regions discussed in Fig S2 and S3 are approximately drawn in c) part. Scale bar is common for the whole image.

Interestingly, the middle copper part is not represented here as a relatively thin and distinct layer but as a layer with some inclusions (Figure S3a,b - region 3). Also region 1 is not fully developed on one substrate side due to the asymmetric substrate position inside of the quartz tube – one side was oriented to the bigger space. As a result, the growth of nanostructures was richer and more developed on one side than on the other one.

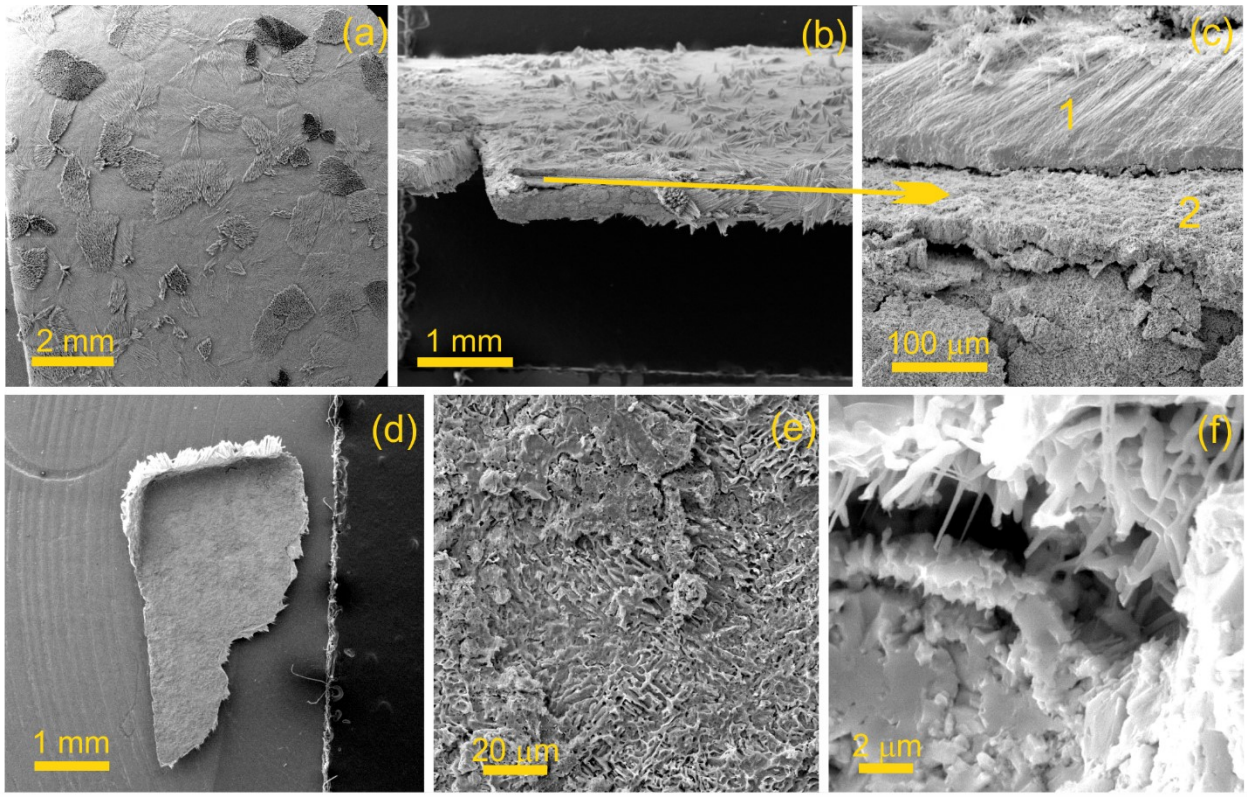

Figure S8 - A gray-black deposit grown onto 0.5 mm Cu substrate` a) horizontal and b) tilt view, c) detail of the peeled off, bare area with visible surface objects (region 1) and spongy part beneath (region 2), d) macroscopic corner piece peeled off the sample, e) morphology of the inner surface of the piece and f) nanostructures on the inner surface in greater magnification.

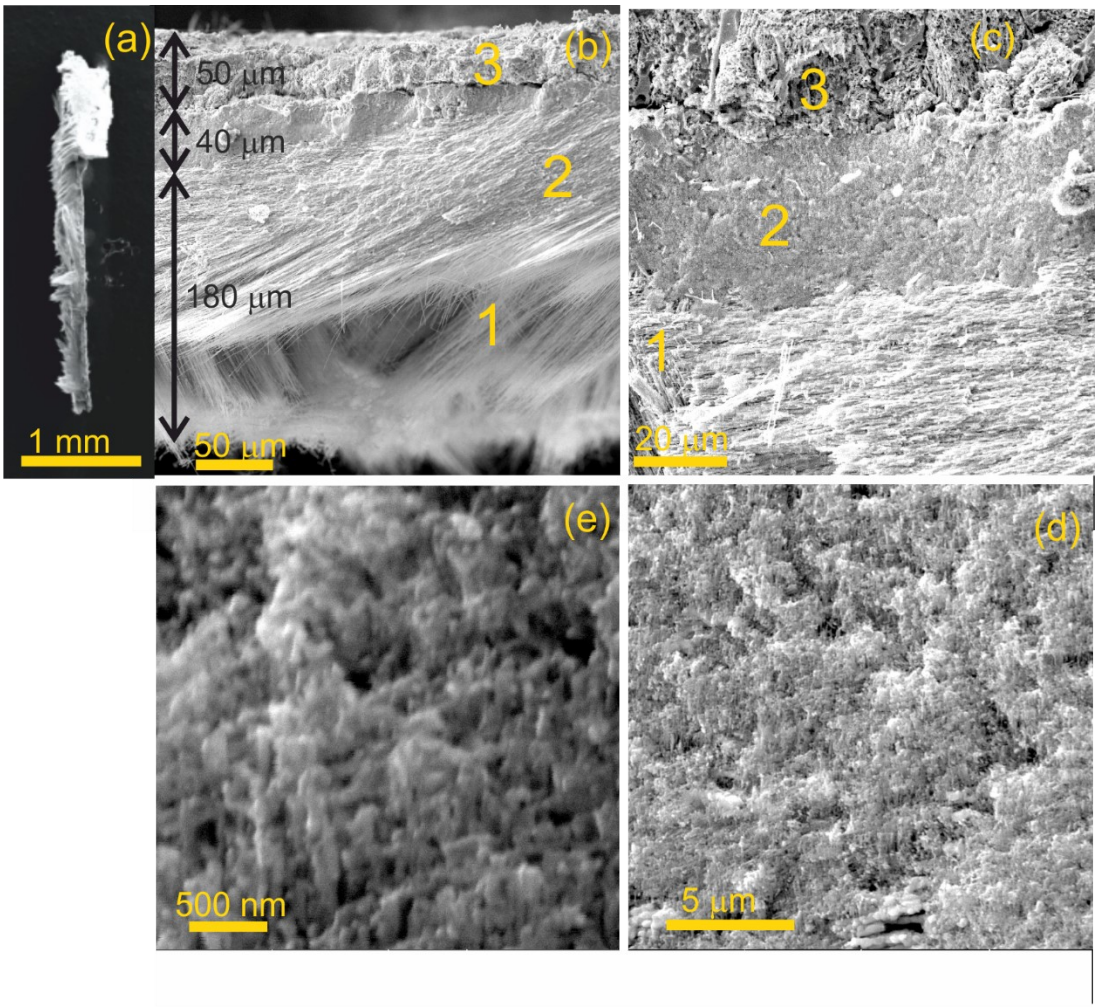

Figure S9 – Peeled off, corner piece of the gray-black sample prepared at 0.5 mm copper substrate – a) overall, side view of the piece (horizontal view of the piece on the Figure S5d), b) cross-section of the piece with indicated thicknesses of appropriate regions: surface object layer (180 µm), porous, sponge-like layer (40 µm) and fragment of the central copper part (50 µm), c) detail of the cross-section – the horizontal orientation of the surface object layer (the lowest located layer) and d, e) details of the porous sponge-like layer in greater magnification are evident. The approximate thickness of catalysis driving material is (2x(180+40))~440 µm. The cross-section b) represents a half of the whole cross-section.

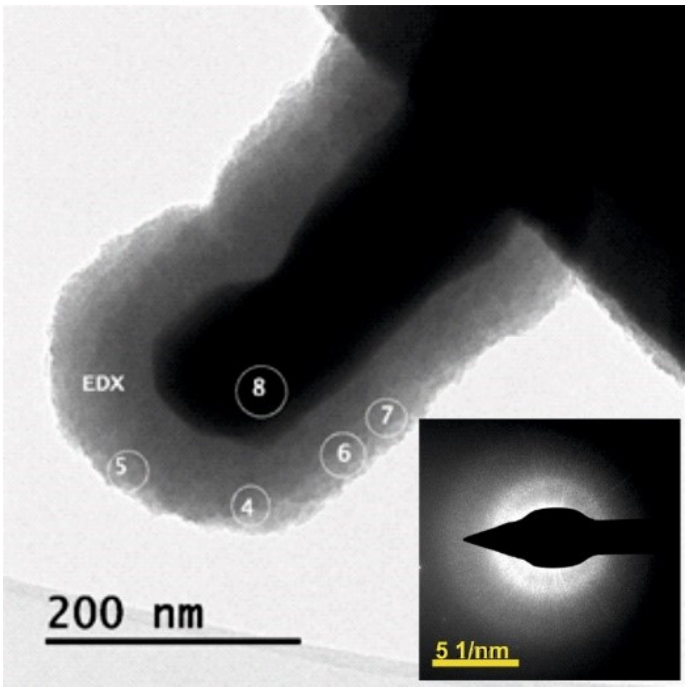

Figure S10 – Spectroscopic characteristics of NR of the bluish sample; location of EDS spots on NR is highlighted (4-8). Spots 4-7 were selected on the shell of NR. Composition in spot 5 is significantly different from spots 4,6 and 7 due to the sample detector geometry (for spot 5 the significant absorption is present). The spot 8 comprises the core of NR as well as the shell. Unlike NR, the covering is from SiC_x (Table S1). Inset is a SAED pattern of the shell revealing its amorphous nature.

Spot / Elemental atomic concetration [%]	4	5	6	7	8
Carbon	46.74	18.72	48.61	48.64	15.03
Silicon	47.73	74.29	44.62	44.09	30.40
Copper	0.20	1.32	1.09	1.43	51.97
Oxygen	5.31	5.65	5.65	5.82	2.58

Table S1 - Atomic concentration at selected spots of NR

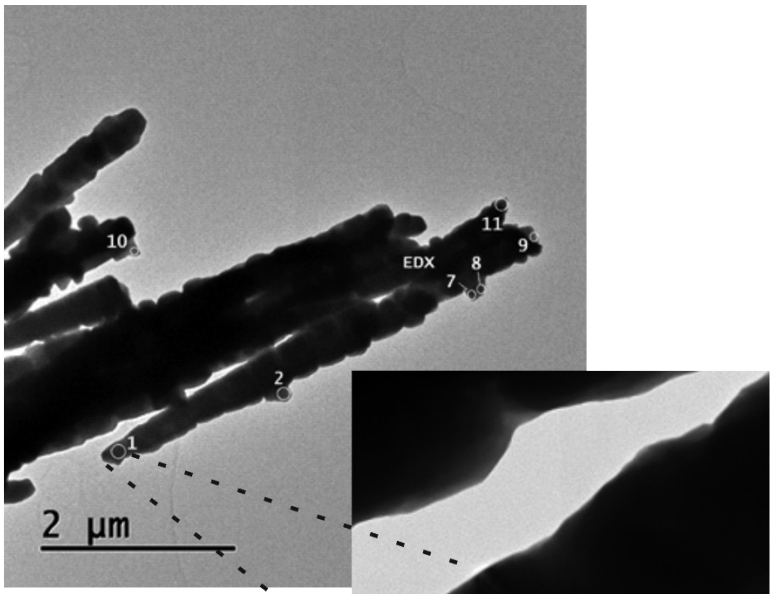

Spot	[Cu]/[Si] ratio
1	3.45
2	2.91
7	2.89
8	2.36
9	2.34
10	4.37
11	2.79

Figure S11 – Bundle of NRs with EDX [Cu]/[Si]molar ratio for the gray-black sample. The analyzed spots represent the peripheries of NRs in order to prove the absence of the SiC_x shell.

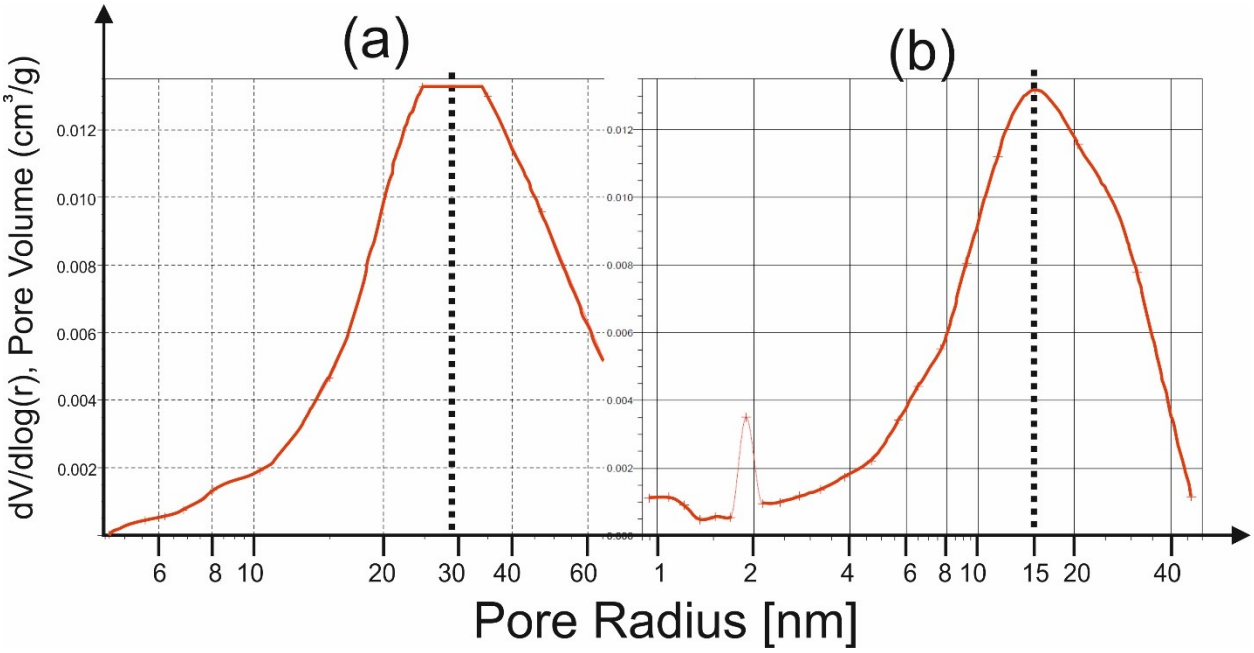

Figure S12 – Nitrogen physisorption measurement yields desorption pore volume for a) gray-black and b) bluish sample with maximum of pore radius at about 30 and 15 nm, respectively.

XPS peak [eV]	Bluish deposit[a)]	Gray-black deposit[a)]	Cu_5Si (standard)[b)]	Assignment	Ref.
Si 2p	99.58	99.23	99.45	Si-Cu, Si^{+0}	[3, 4]
	100.3	100.07	100.36	Si-C, Si^{+1} (Si_2O)	[1, 4]
	101.5	101.33	--	Si^{+2} (SiO)	[4]
	102.5	102.52	102.18	Si^{+3} (Si_2O_3)	[4]
	103.5	103.86	103.38	Si^{+4} (SiO_2)	[4]
Cu $2p_{3/2}$	--	931.77	932.03	Cu^{+1}	[2]
	~933w	933.27	932.96	Cu-Si, Cu^{+0}	[2, 5]
	--	934.61	933.67	$Cu(OH)_2$, Cu^{+2}	[2]
C 1s	283.0	283.0	--	C-Si	[1]
	284.76	284.47	284.80	C-H, C-C (adventitious	[6, 7]
	285.72	285.97	286.04	carbon)	[6, 7]
	287.17	--	--	C-O-C	[6, 7]
	289.39	--	--	O-C=O	[7]
O 1s	532.21	532.0	532.49	O-Si-O (silicone), Si^{+2} (SiO)	[4, 6]
	--	533.07	--	O-C-O, O-(C-O)-O	[8]
	533.8	--	--	O-(C=O)-C, Si^{+4} (SiO_2)	[4, 8]

[a)] after 180 sec Ar^+ sputtering 1 kV, [b)] after 360 sec Ar^+ ion sputtering 1 kV, w - weak

Table S2 – XPS data of chemical shifts of Si, Cu, C and O in prepared deposits and Cu_5Si standard. The XPS peaks were deconvoluted into subpeaks, which correspond to specific chemical species according to refs.

[1] X-ray Photoelectron Spectroscopy (XPS) Reference Pages http://www.xpsfitting.com/search/label/Silicon (accessed Jan 26. 2024)

[2] X-ray Photoelectron Spectroscopy (XPS) Reference Pages http://www.xpsfitting.com/search/label/Copper (accessed Jan 26. 2024)

[3] Y. Samson, B. Tardy, J. C. Bertolini, G. Laroze, *Surf. Sci.* **1995**, *339*, 159-170. https://doi.org/10.1016/0039-6028(95)00573-0

[4] R. Alfonsetti, L. Lozzi, M. Passacantando, P. Picozzi, S. Santucci, *Appl. Surf. Sci.* **1993**, *70/71*, 222-225. https://doi.org/10.1016/0169-4332(93)90431-A

[5] F. Ringeisen, J. Derrien, E. Daugy, J. M. Layet, P. Mathiez, F. Salvan, *J. Vac. Sci. Techmol B* **1983**, *1*, 546-552. https://doi.org/10.1116/1.582596

[6] https://www.thermofisher.com/cz/en/home/materials-science/learning-center/periodic-table/non-metal/carbon.html (accessed Jan 26. 2024)

[7] http://www.xpsfitting.com/search/label/carbon (accessed Jan 26. 2024)

[8] http://www.xpsfitting.com/search/label/Oxygen (accessed Jan 26. 2024)

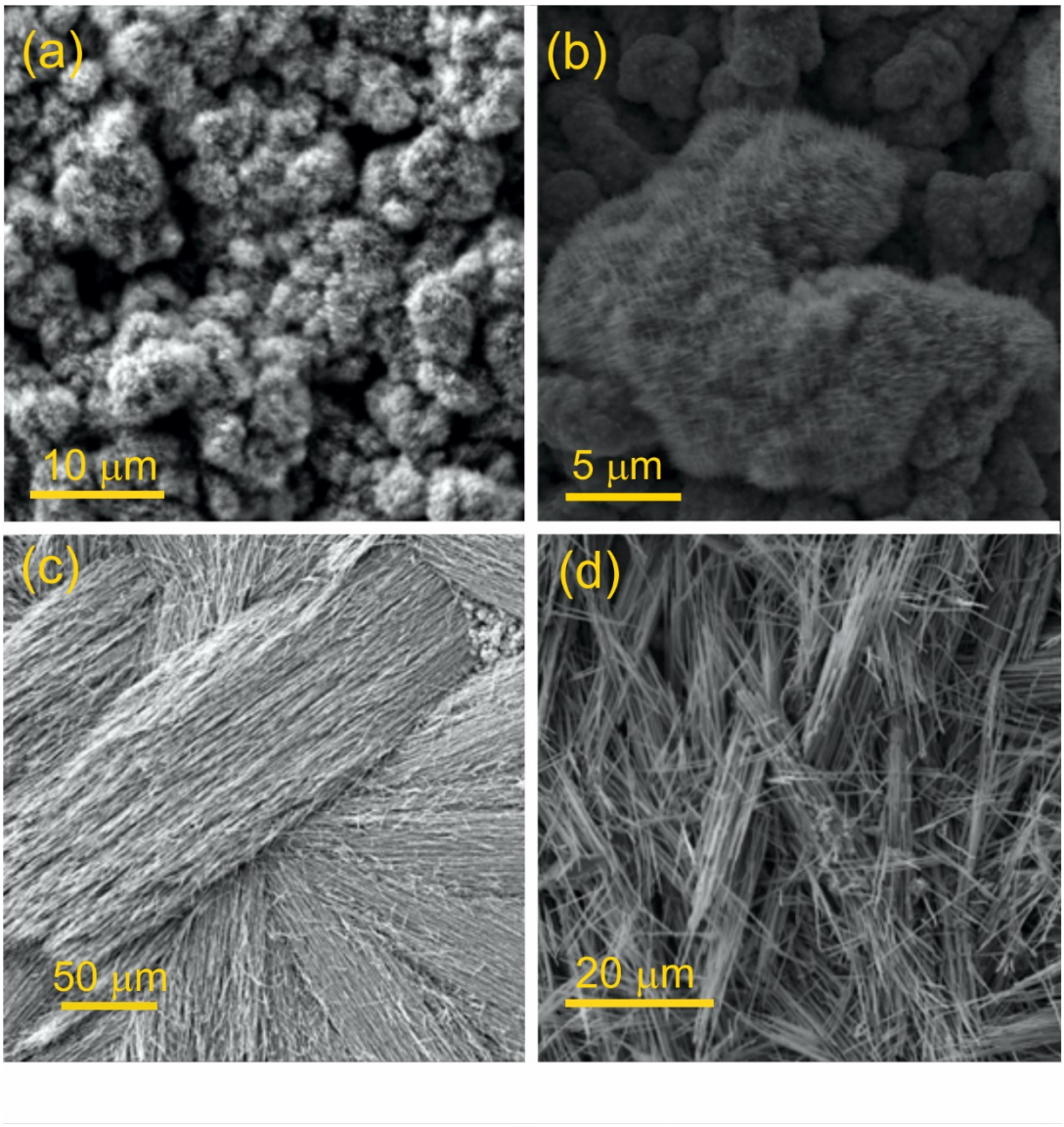

Figure S13 – Comparison of various morphologies before (a ,c)) and after (b, d) electrochemical experiments (gray-black sample)

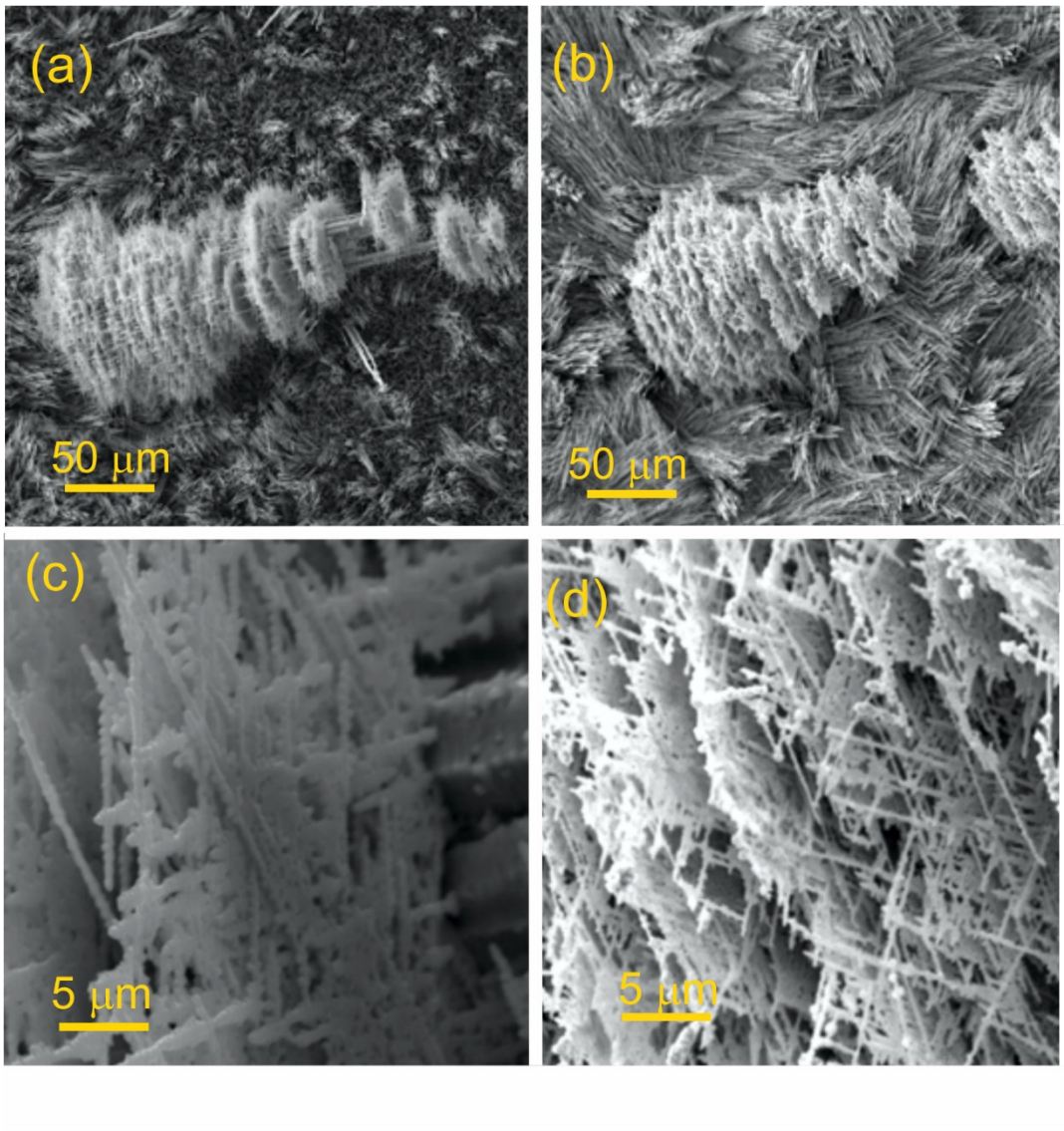

Figure S14 – Comparison of various morphologies before (a ,c)) and after (b, d) electrochemical experiments (bluish sample)

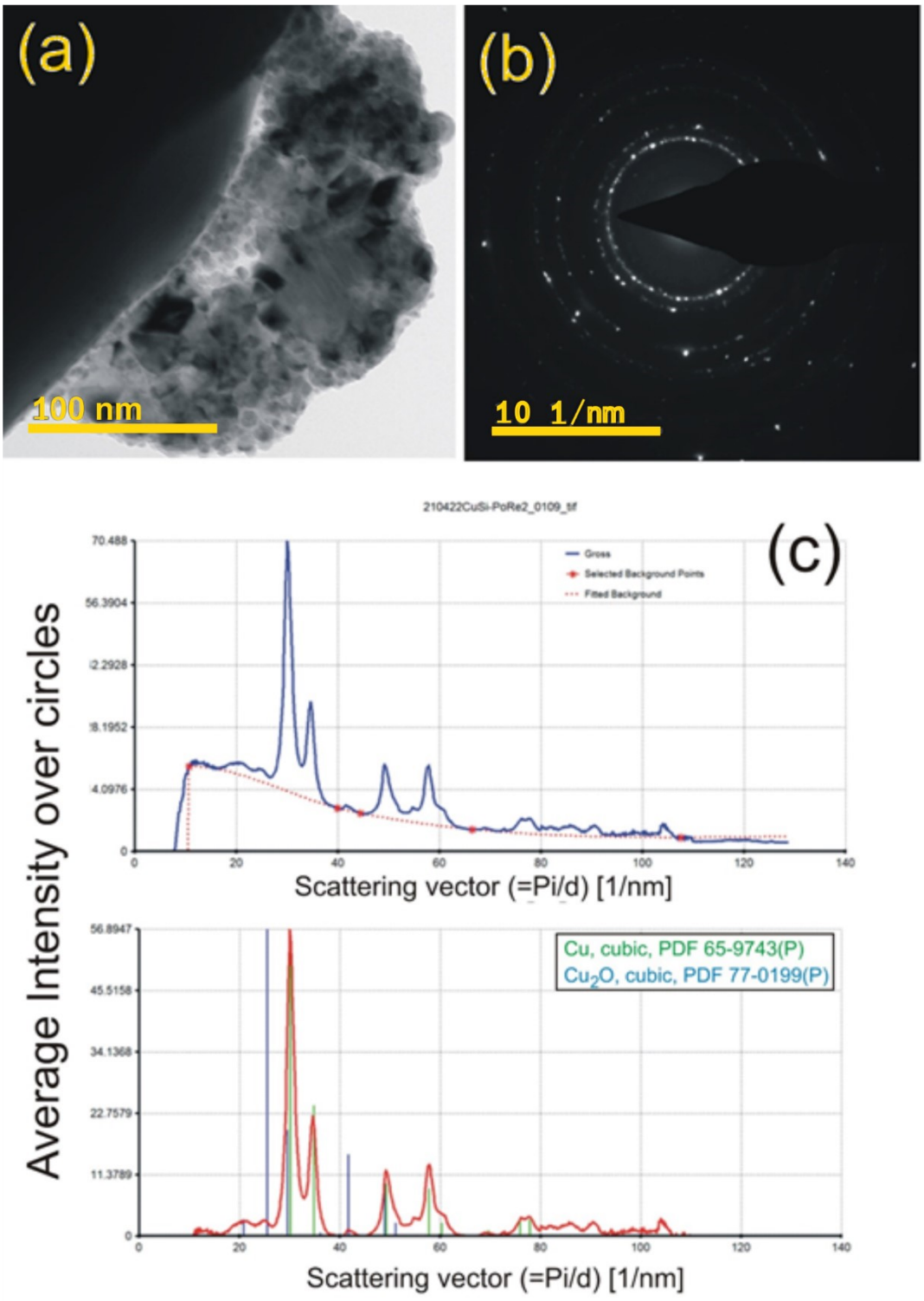

Figure S15 – (a) HRTEM image of the thin nanoleaf and (b) its ED, (c) average intensity over circles of the ED pattern (b). The upper picture and lower picture in (c) is before and after background subtraction, respectively.

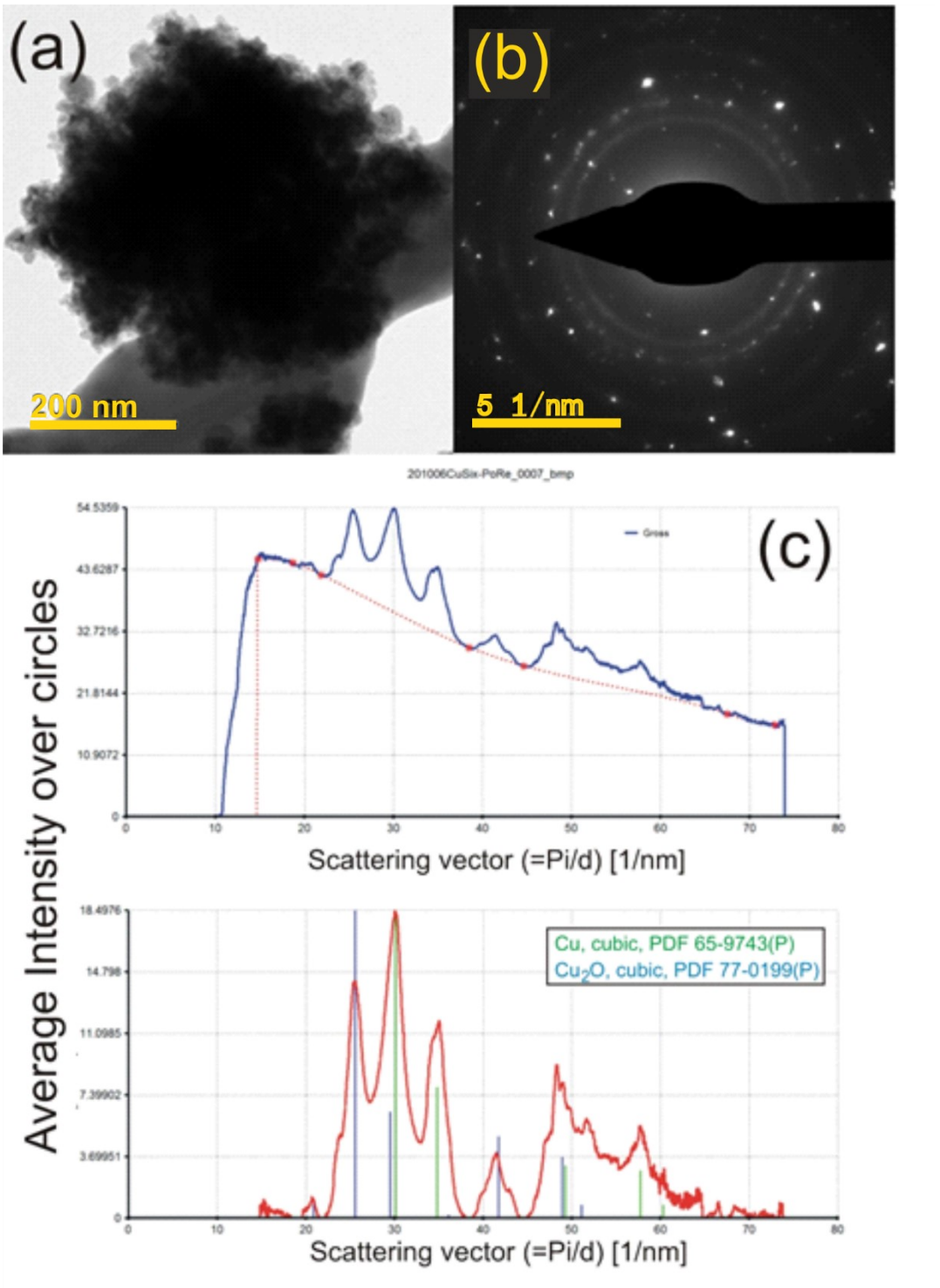

Figure S16 – a) HRTEM image of the (thick) nanoflower and (b) its ED, (c) average intensity over circles of the ED pattern (b). The upper picture and lower picture in (c) is before and after background subtraction, respectively.

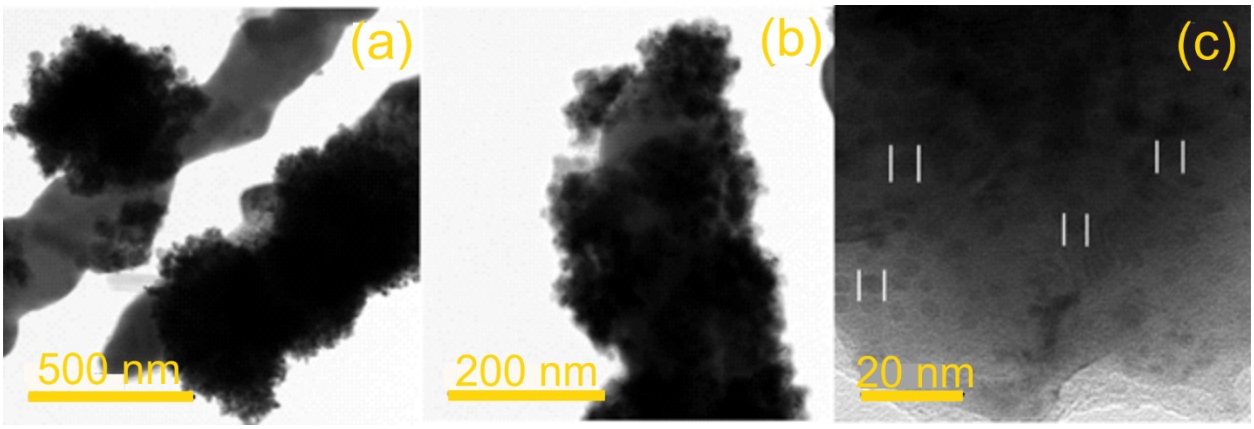

Figure S17 – TEM images in low and high magnification showing large nanocrystalline overgrowths in the (a) bluish and (b) gray-black samples. A close detail (c) of such nanocrystalline overgrowth in a gray-black sample. Globular nanocrystals are clearly observable in the surrounding matrix. Some of them are marked out.

Potential applied vs RHE [V] →	-0.6	-0.55	-0.4
Acetate/Ethanol (pH 10.3)	0.72/0.08	0.43/0.09	0.23/0.09
Acetate/Ethanol (pH 6.79)	0.06/0.79	0.07/0.47	0.08/0.25

Table S3 - eCO_2RR product composition as function of pH and applied potential for bluish sample

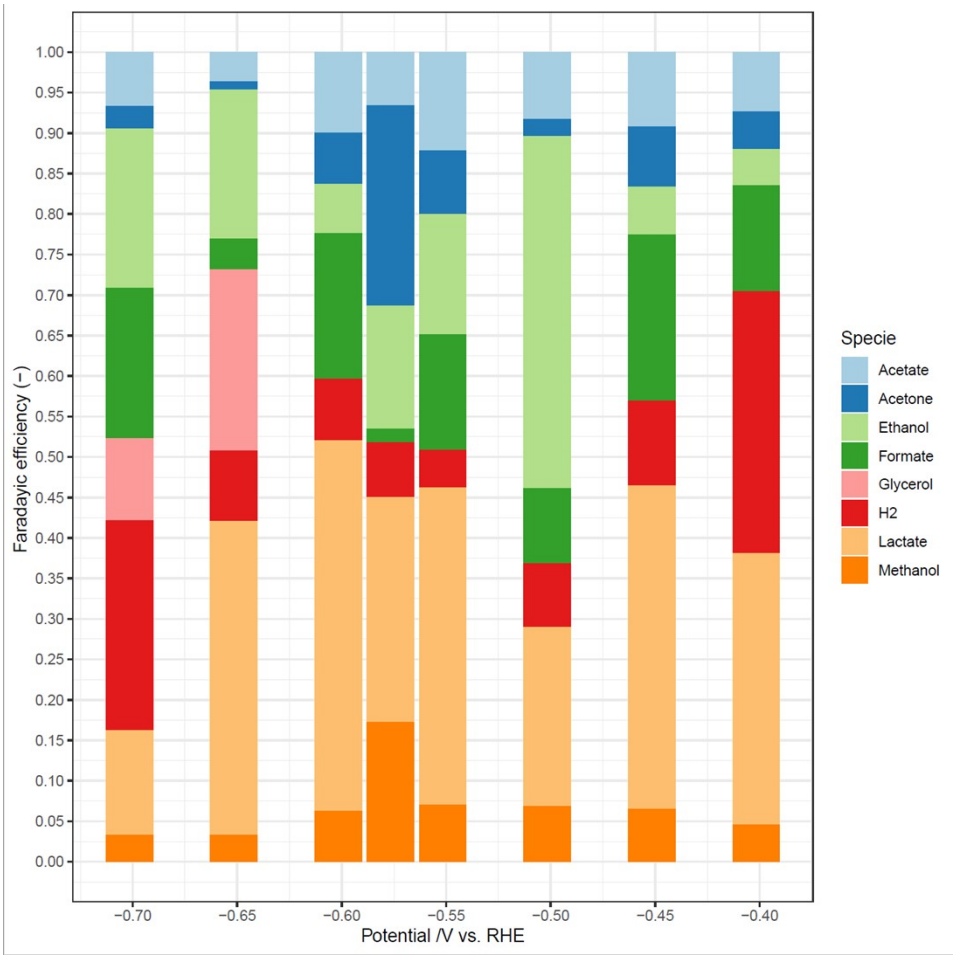

Figure S18 - eCO_2RR product composition as function of applied potential for gray-black sample.

Note: Observed concentrations for gray-black sample in NMR and GC-MS were smaller than for bluish sample, the Figure S18 therefore represent only the "preview" of formed eCO_2RR products as function of applied potential.

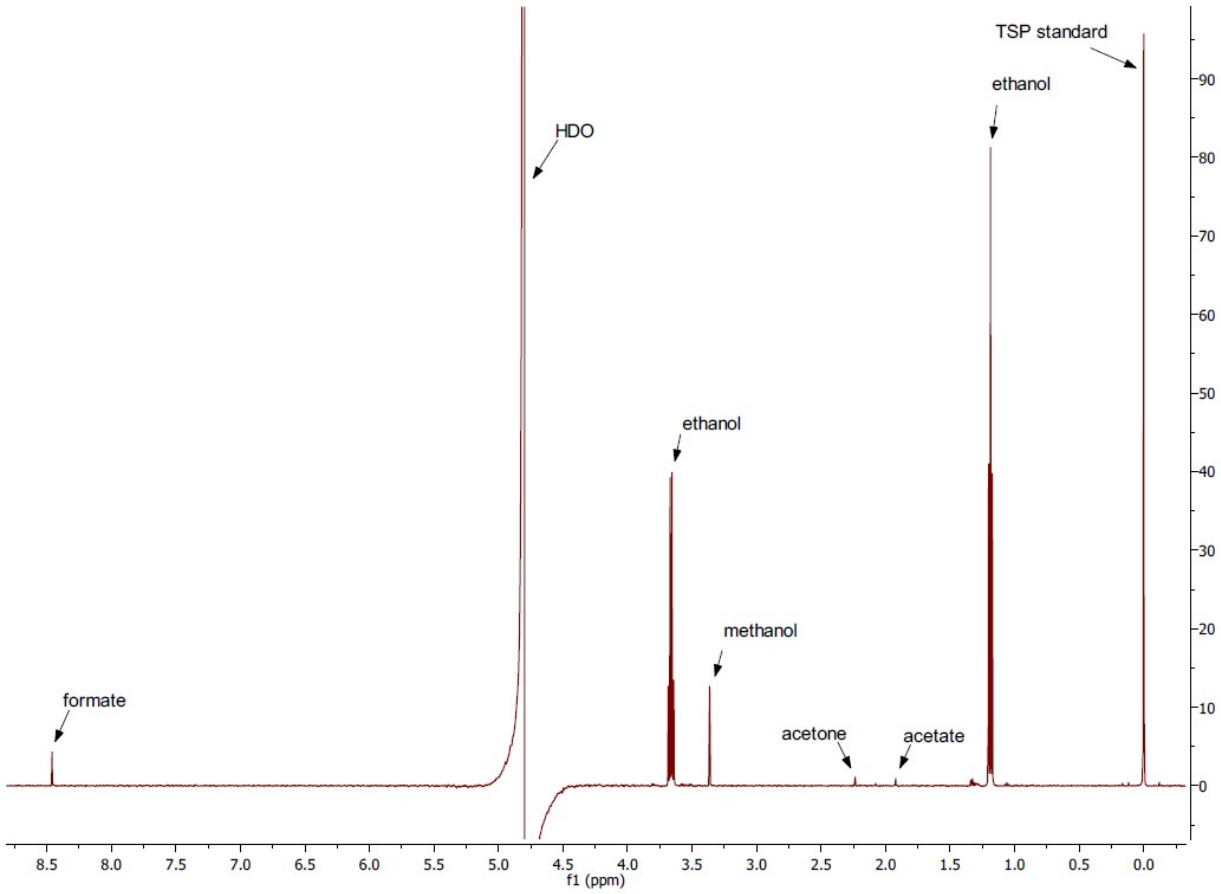

Figure S19 – NMR spectrum of products for bluish sample at maximum FE

The integrated concentrations of individual peaks in Figure S19 are listed below:

Compound Name	Concentration (mg/dL)
Ethanol	5,8918
Formate	0,4491
Methanol	0,3479
Acetate	0,0418
Acetone	0,0278